Reinforcement of Polyamide 6 with Nanoparticles

*Luis F. Giraldo, Mauricio Echeverri, Betty L. López**

Polyamide 6 has been reinforced by in situ polymerization of ε-caprolactam by using either 2 wt % of multiwall carbon nanotubes of two different diameters and length or 2 wt % functionalized nonporous Stöber silica. The carbon nanotubes were synthesized by catalytic chemical vapor deposition of ethylene over two different supports: iron particles supported on MCM41 mesoporous silica and iron-cobalt particles on $CaCO_3$, in order to produce multiwall carbon nanotubes with average diameter of 32 and 58 nm respectively. The Stöber silica particles with diameters of 85 nm and 150 nm were functionalized with 3-aminotrimethoxypropyl silane. The thermal stability of nanotubes/Polyamide 6 nanocomposites increases compared to the neat polyamide 6, and this increase is even larger when the functionalized silica nanoparticles are used as a filler. The crystallinity of polyamide is enhanced when carbon nanotubes are functionalized, but it decreases with or without functionalization of the silica particles. The nanotubes increase the temperature of crystallization in the nanocomposites due to the reduction in the mobility of polymer chains.

Keywords: Carbon nanotubes; Polyamide 6; Reinforcement; Silica nanoparticles

Introduction

The nanoparticles are without doubt one of the most outstanding and promissory fillers that are being studied by many scientists all over the world, due to their high surface area, low density and high young's modulus, among other properties that can be transferred to the polymeric matrix if a good dispersion of the filler is ensured in the polymer. One of the most studied nanomaterials is the carbon nanotubes, because of their extraordinary mechanical and unique electronic properties. The carbon nanotubes can be produced by means of different techniques, being the catalytic chemical vapor deposition (CCVD) the most versatile and promising method of synthesis to be applied to industrial scale. In this technique the diameter of nanotubes is mainly affected by the size and nature of the catalytic metal particles, and their interaction with the support.[1–5]

On the other hand, the polyamide 6 (PA6) is one of most important polymers used not only in the textile industry, but also in other industrial applications where tribological properties are crucial due to its higher wear resistance in relation with other polymeric fibers.[6–8]

The reinforcement of this polymer has been studied with layers of silicate and carbon nanotubes as filler agents.[9–15] However, most of those reinforcements have been carried out by melt-mixing and only few of them are made by in-situ polymerization.[16–18]

In this work, we make a comparative study of the thermal stability of PA6 reinforced with 2 wt % of multiwall carbon nanotubes (MWCNTs) and 2 wt % silica nanoparticles. The MWCNTs were synthesized in our laboratory by catalytic chemical vapor deposition of ethylene on iron dispersed on mesoporous sílica MCM41 and iron/cobalt on calcium carbonate. The silica particles were synthesized by means of the Stöber method, which consists in the

Grupo Ciencia de los Materiales, Sede de Investigación Universitaria (SIU), Universidad de Antioquia, Calle 62 # 52-59 Torre 1 Laboratorio 310-311 Medellín, Colombia
Tel: (+574) 2106545 Fax: (+574) 2106550
E-mail: blopez@quimbaya.udea.edu.co

polycondensation of tetraethylorthosilicate (TEOS) in an ethanolic medium catalyzed with ammonia in order to form nonporous spherical silica particles.[19–22] This procedure was carried out at two different temperatures in order to produce silica particles with different sizes. We have studied the influence of functionalization of carbon nanotubes and silica on the thermal and crystalline properties of nanocomposites, as the effect of the in-situ reinforcement by polymerization of ε-caprolactam, grafting the filler to the monomer.

Experimental Part

Materials

The ε-Caprolactam (99%), 6-aminocaproic acid (99%), 3-Aminopropyltrimethoxysilane (97%), ammonium hydroxide (NH_3 28%) were purchased from Sigma Aldrich, hydrofluoric acid (40 %), iron (III) nitrate nonahydrated, 27% sodium silicate solution and Toluene (99.9%) from Merck. TEOS (98%) and cetyltrimethylammoniumbromide (99+%) from ACROS Organics, Ethanol anhydrous reagent (MP Biomedicals).

Synthesis of Catalysts

The Fe (6%)/MCM41 and Fe(6%)-Co(12%)% $CaCO_3$ catalysts were prepared by impregnation method.[23,24]

The mesoporous silica was prepared using sodium silicate as silica source and cetyltrimethylammoniumbromide (CTMABr) as template. CTMABr (2.8 g) is dissolved in 10.0 mL HCl (1M) and 15.0 mL of water at 30 °C under magnetic stirring by 30 min. After which 6.0 g of sodium silicate (dissolved in 30,0 mL the water) are added (pH = 9.8–10). The final gel is kept at 100 °C for 72 hours in an autoclave covered with Teflon. The solid is recovered by filtration, dried at 60 °C and calcined in air at 540 °C by 3h.

Synthesis of MWCNTs

The syntheses of MWCNTs were carried out by means of catalytic chemical vapor deposition of ethylene at 750 °C by using the former catalysts.

In a typical synthesis 1,0 g of catalyst is placed inside of an ''U''-shaped quartz and heated up to 750 °C in nitrogen atmosphere, then the ethylene at 300 cm^3/min is diluted in nitrogen at 100 cm^3/min and flowed through the tube for 30 minutes. After, the furnace is cooled down to room temperature the product is removed. When iron is deposed on mesoporous silica, a previous reduction of the catalyst is carried out with 50 cm^3/min of H_2 in 150 cm3/min N_2 for 15 minutes.

The purification of the material is carried out using hydrofluoric acid at 20% in order to eliminate the silica support and the metal particles, in the case of calcium carbonate the purification is done with nitric acid at 30%. The carbon nanotubes are filtered and washed with water, and dried at 100 °C over night.

Functionalization of MWCNT

The functionalization of MWCNTs was carried out by treatment with nitric acid at 30% for one night under reflux, after that the samples were washed with distilled water and dried at 120 °C over night.

Synthesis of Silica Nanoparticles

85 nm and 150 nm spherical silica particles were synthesized by the Stöber method at two different temperatures. For the first ones, 100 mL of absolute ethanol and 7,5 mL of an aqueous solution of ammonium (28%) was introduced in a two-neck 250 mL round flask equipped with a refrigerating system. The mixture was stirred at 300 rpm and heated up to 60 °C. Then, 3,0 mL of TEOS was introduced to the solution and the reaction was held during 24 h under permanent stirring. The 150 nm silica particles were synthesized through a similar procedure, but at room temperature.[25]

For the silica functionalization, 1,0 g of each silica was dispersed in 30 mL of dry toluene and treated with 1 mL of 3-aminopropyltrimethoxysilane (AMPS) during 24 hours under reflux. Then, the crude

products were collected, washed five times with dry toluene, ethanol and water, and then dried at 150 °C for 24 h.[26]

Synthesis of PA6

The polyamide 6 was synthesized by ring opening polymerization of ε-caprolactam using 6-aminocaproic acid like initiator. 20 g of ε-caprolactam was placed in a three necked flask. Then, the carbon nanotubes or the silica particles were mixed in concentration of 2 wt % with the monomer for one hour at 100 °C, then 2 g of 6-aminocaproic acid was added and the temperature of the reaction system was increased until 250 °C, and left a this temperature for 5 hours with mechanical stirring at 300 rpm.

After the reaction was stopped, the polymer was washed with boiling water at least three times. Then, the materials were dried at 120 °C over night.

Thermal Analysis

DSC analyses were made in a Q100 calorimeter from TA Instruments. The PA6 and nanocomposites were heated at 250 °C and held during one minute at this temperature, and then the samples were cooling to 25 °C, and heated again at 10 °C/min until 250 °C and held during one minute at this temperature, after the non-isothermal crystallization was carried out cooling the sample at 20 °C/min until 25 °C.

The thermogravimetric analyses of nanocomposites were made with a Q500 TA instrument in air atmosphere at 10 °C/min up to 700 °C. In the case of carbon nanotubes, the final temperature was 800 °C at the same rate.

Microscopic Analysis

The carbon nanotubes were placed in 5 mL of absolute ethanol and sonicated for 20 minutes. A drop from the suspension was placed on a 200-mesh copper grids coated with Formvar as sample support. Samples were viewed and photographed using a Tecnai 20 TW, FP 5020/10 Phillips Transition Electron Microscopy. SEM micrographs were taken in a JEOL JSM T-300 scanning electron microscope.

XRD

The X-ray analyses were performed at room temperature in a Siemens D5000 equipped with a Cu-Kα source ($\lambda = 1.54$ Å), with a 0.04° step.

FTIR

IR spectra were obtained from FTIR spectrometer Perkin Elmer Spectrum One from KBr pellets.

Figure 1.
SEM and TEM images of MWCNTs synthesized by CCVD of ethylene on Fe/MCM41.

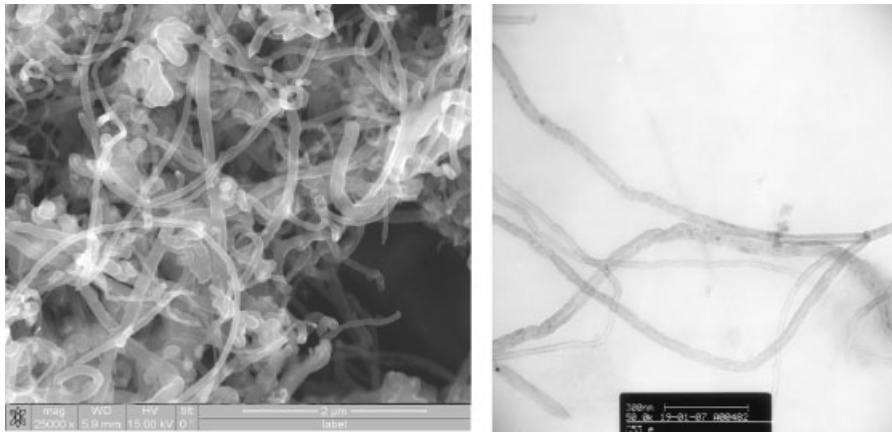

Figure 2.
SEM and TEM images of MWCNTs synthesized by CCVD of ethylene on Fe-Co/$CaCO_3$.

Results and Discussions

Figure 1 shows SEM and TEM images of MWCNTs synthesized by using iron on mesoporous sílica MCM41 as catalyst. The nanotubes obtained have an average diameter of 32 nm and a length larger than 10 μm. The nanotubes produced over Fe-Co supported on $CaCO_3$ (Figure 2) present a broader particle size distribution (42–85 nm), but they are shorter in comparison to the previous ones. The higher surface area of mesoporous silica ensures a better dispersion of the metallic cluster, and this induces the formation of carbon nanotubes of thinner diameter.

Figure 3 shows the sílica particles synthesized by the Stöber method at 60 °C (left) and room temperature with average diameter of 85 nm and 150 nm respectively. The particles have semispherical morphology and they are agglomerated owing to the hydrogen bonds between the silanol groups. The higher process temperature increases the nucleation rate and this makes that the final particle size be reduced.

Figure 4 shows the thermograms of the carbon nanotubes purified by acidic treatment. They present one weight loss around 600 °C, which for the ones synthesized on mesoporous support is sharper and corre-

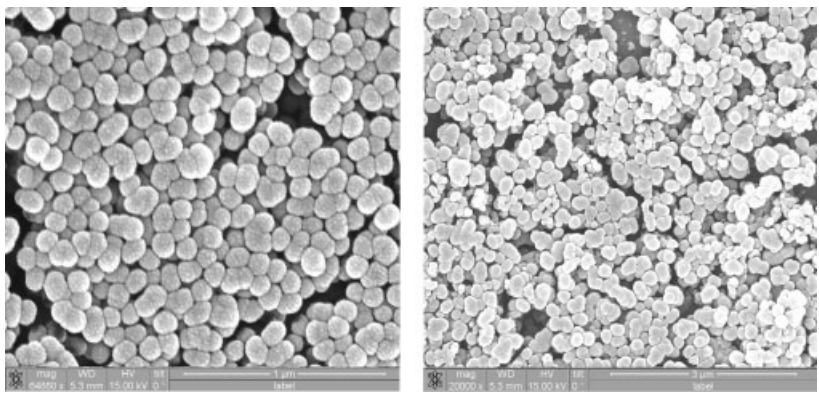

Figure 3.
SEM images of silica particles synthesized by the Stöber method at 60 °C (left) and room temperature (right).

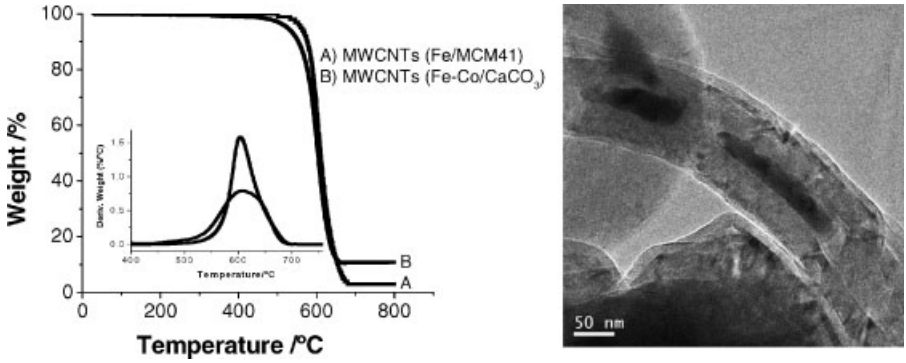

Figure 4.
TGA of MWCNTs synthesized on Fe/MCM41 and Fe-Co/CaCO3 (left). TEM image of nanotubes synthesized by using Fe-Co/CaCO3 (right).

sponds to 98 wt %. In the case of nanotubes synthesized on $CaCO_3$ this loss is around 90 wt%, and its decomposition range is wider. The other 10 wt% corresponds to the metal particles that are inside the carbon nanotubes (Figure 4, right) and still remain after the purification because they can not be eliminated by the acids.

The IR spectra of MWCNTs with and without functionalization are shown in Figure 5 (left). The new bands at 2923 cm^{-1} and 2859 cm^{-1} are assigned to the stretching of saturated C–H. At 1729 cm^{-1} there is a peak associated with the stretching of carbonyl group. Since the open nanotubes contain atoms that are not completely bonded to the cylinder network or five-seven member rings that are presented as structure defects at the ends or in the bending of the nanotube, the more susceptible sites to be functionalized with the acid groups are the nanotubes ends, generating new chemical bonds.

The infrared spectra of silica with and without functionalization are shown Figure 5 (right). In the silica spectrum, the band at 3410 cm^{-1} is attributed to the presence of the O–H-stretching frequency of silanol groups and also to the remaining adsorbed water. The bands at 1096 cm^{-1} and 956 cm^{-1} are related to Si–O stretching frequencies of the silica.

The silica functionalized with AMPS presents the same peaks than the previous

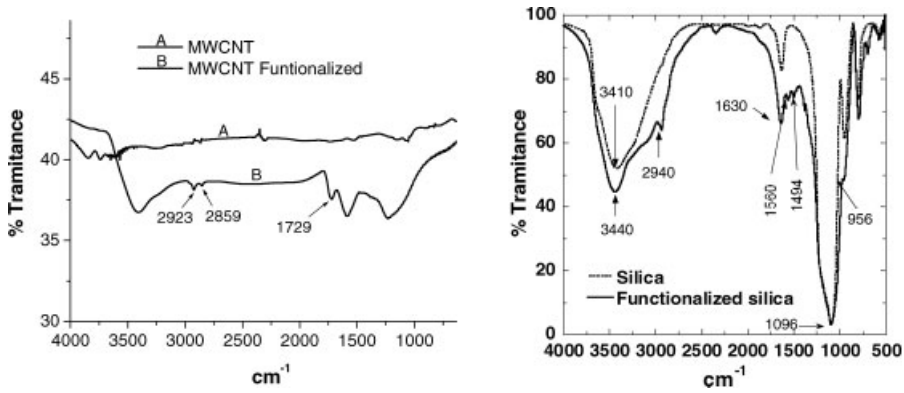

Figure 5.
FTIR spectra of MWCNTs functionalized by acid treatment (left) and silica particles functionalized with AMPS.

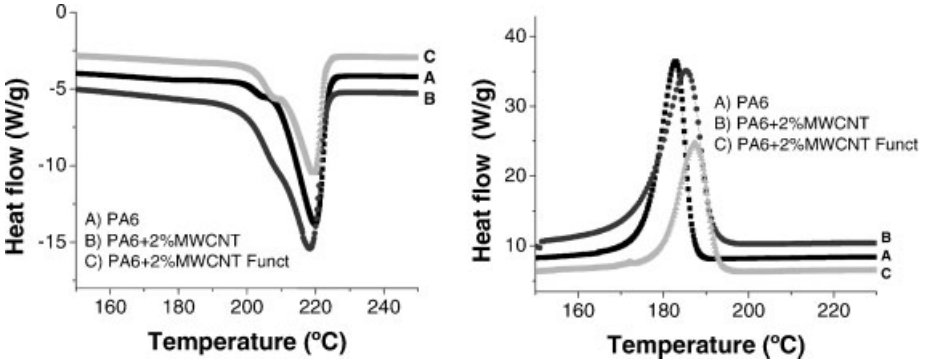

Figure 6.
DSC thermograms of melting (left) and non-isothermal crystallization (right) of PA6 + 2 wt % MWCNTs synthesized on $CaCO_3$ with and without functionalization.

Table 1.
Values *of* T_c, T_m, $\Delta_m H$, X_c for PA6 and MWCNTs and silica/PA6 composites.

Sample	T_c (°C)	T_m (°C)	$\Delta_m H$ (J/g)	X_c^a (%)
PA6	182.8	219.8	56.3	23.4
PA6 + MWCNT/$CaCO_3$	185.7	219.1	56.5	23.5
PA6 + MWCNT/$CaCO_3$ Funct	187.6	219.5	61.5	25.6
PA6 + MWCNT/MCM41	187.9	219.9	55.2	23.1
PA6 + MWCNT/MCM41 Funct	183.7	219.6	56.8	23.7
PA6 + 2% Silica (85)[b]	180.3	219.2	51.9	21.6
PA6 + 2% Silica (85) Funct	177.4	218.2	53.3	22.2
PA6 + 5% Silica (85) Funct	175.7	217.2	45.9	19.1
PA6 + 2% Silica (150) Funct	176.3	215.7	46.3	19.3
PA6 + 5% Silica (150) Funct	176.1	216.3	43.4	18.1

[a] Calculated as the relation between the $\Delta_m H$ and $\Delta_m H^\circ$ (240 J/g), $\Delta_m H^\circ$ corresponds to the average between the crystalline phases γ and α.
[b] Silica particles of average 85 nm without functionalization.

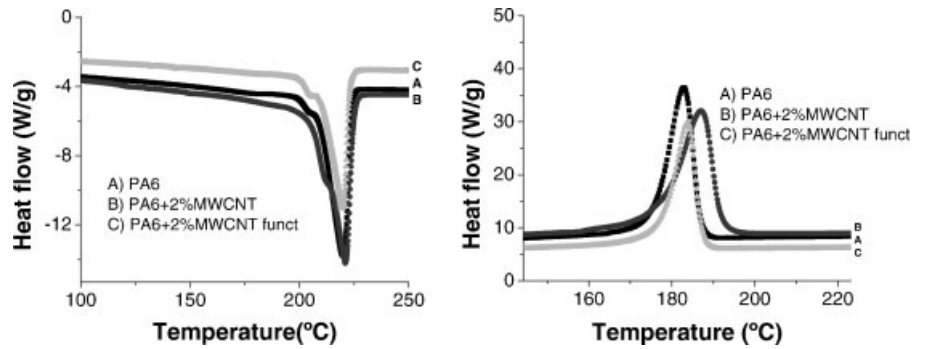

Figure 7.
DSC thermograms of melting (left) and non-isothermal crystallization (right) of PA6 + 2 wt % MWCNTs synthesized on MCM41 with and without functionalization.

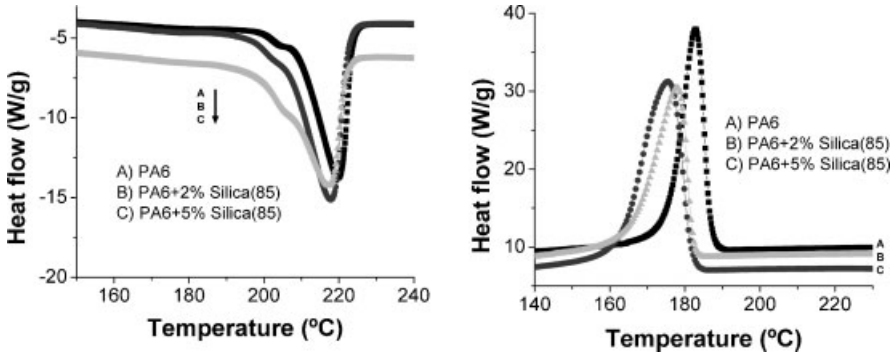

Figure 8.
DSC thermograms of melting (left) and non-isothermal crystallization (right) of PA6 + 2 wt % Silica nanoparticles synthesized at 60 °C and functionalized with AMPTS.

spectrum and also there are weak bands at 2940 cm^{-1} and 1494 cm^{-1} due to C–H stretching and bending, respectively. That confirmed the attachment of the organic molecule on the silica surface. The change of the band shape around 3440 cm^{-1} is assigned to the presence of the amino groups, and this is confirmed by the peak at 1560 cm^{-1}, the bending mode of N–H groups, and the band at 1494 cm^{-1} which indicates the presence of alkyl groups.

The DSC thermograms for PA6 reinforcement with MWCNTs/$CaCO_3$ are shown in Figure 6. The melting temperature of PA6 is practically unaltered, but $\Delta_m H$ increases as it is shown in Table 1. For the non-isothermal crystallization of the nanocomposites shown in Figure 6 (right), it is interesting to note that the crystallization temperature increases with the addition of nanotubes and this increase is even more pronounced when the polymer is reinforced with functionalized MWCNTs due to better dispersion and grafting of the filler with the polymeric matrix, reducing the mobility of the polymeric chains, as it has been suggested by different authors than have obtained an increase in Tg for PA6 reinforced with several fillers measured by dynamic mechanical analysis.[16,27] Figure 7 shows the DSC thermograms for PA6 reinforced with MWCNTs/MCM41. In this case the $\Delta_m H$ slightly increases when functionalized carbon nanotubes are added, the crystallization temperature also increases, but the nanotubes without functionalization cause a higher increase in Tc, in contrast to the previously observed

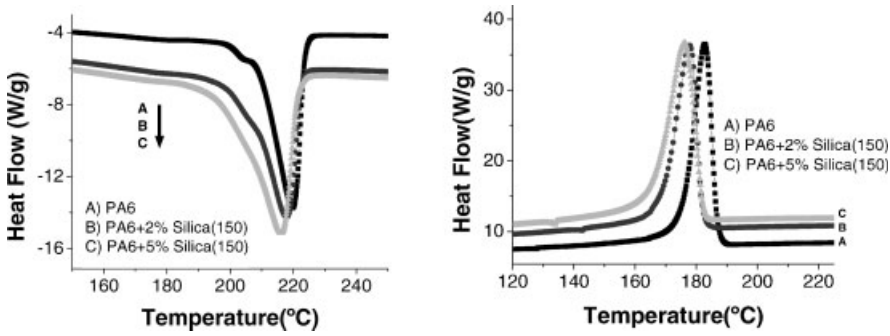

Figure 9.
DSC thermograms of melting (left) and non-isothermal crystallization (right) of PA6 + 2 % Silica nanoparticles synthesized at room temperature.

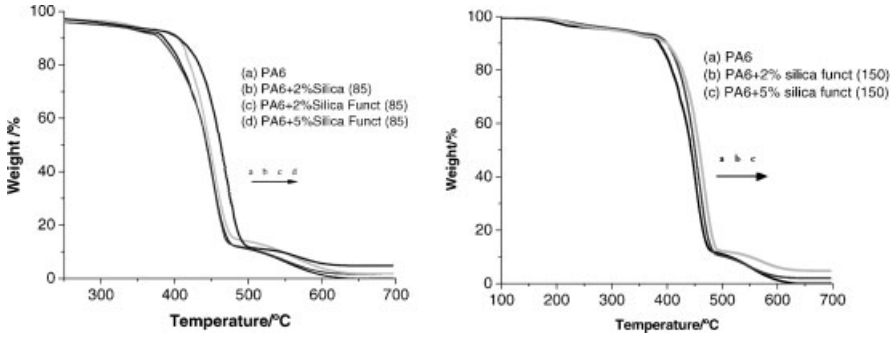

Figure 10.
TGA thermograms of PA6 + 2 and 5 wt % of silica of 85 nm (left) and 150 nm (right).

behavior of PA6 reinforced with MWCNTs/$CaCO_3$. This can be explained because the carbon nanotubes synthesized on mesoporous silica are very long and therefore tend to entangle and agglomerate when they are functionalized owing to the presence of not only for van-der-Waals forces, but also hydrogen bonds to the sidewalls of carbon nanotubes.

Contrary to the carbon nanotubes, the silica filler reduced the crystallization temperature of PA6 as shown in Figure 8 and 9. The degree of crystallization and melting temperature are also reduced, and this reduction is higher for the silica particles of larger particle size as shown in Figure 9. Because of its morphology, the silica particles can disrupt the lamellar organization and the folding of the polymer chains, causing a limited diffusion and alignment of PA6 chains and therefore reduce the crystallinity.

The TGA analysis of PA6 reinforced with silica is shown in Figure 10. As the concentration of silica increases, the degradation temperature of PA6 increases, and this effect is even more significant when the silica nanoparticles are functionalized and the silica concentration is 5 wt %. There is an interesting increase in the degradation temperature of nanocomposites reinforced with the small-sized nanoparticles. In the

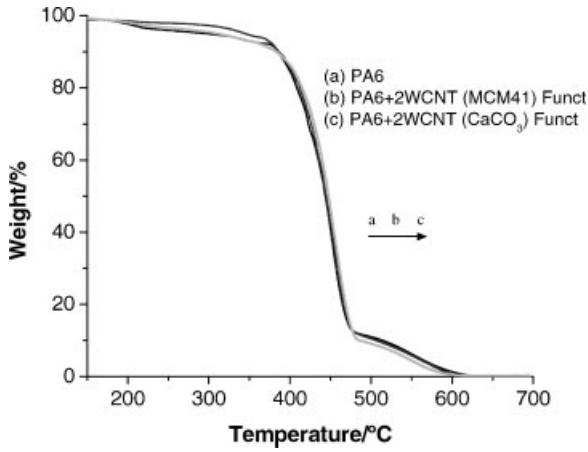

Figure 11.
TGA thermograms of PA6 + 2 wt % functionalized MWCNTs with different diameters.

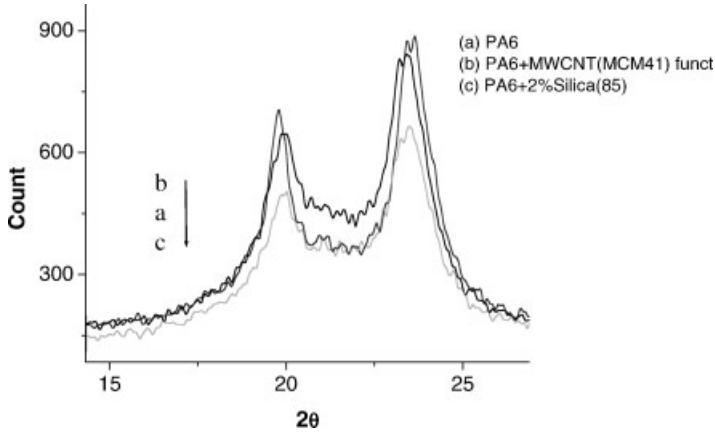

Figure 12.
XRD patterns of PA6 with carbon nanotubes and silica at 2 wt%.

case of carbon nanotubes (Figure 11) the thermal stability of nanocomposites is just slightly increased when the carbon nanotubes are functionalized. This effect can be for the better diffusion of oxygen through the polymeric matrix which is hindered in the case of silica nanoparticles, delaying the degradation of PA6.

The XRD patterns for PA6, and PA6+ MWCNTs and PA6+ silica nanocomposites show the same crystalline phase. The α crystalline form is identified by the peaks at approximately at $2\theta = 20$ and 23,7°. It is interesting to note that the XRD patterns are different from those observed when the polyamide is reinforced with nano clays like montmorillonite, which induce the formation of γ-phase crystals, as it is reported in several studies,.[9,10,28] It has been proposed that the presence of 2D layers in the clay disrupts the α-crystallite formation and results in the less ordered γ-phase crystals.

In our case all the nanocomposites maintained the α-crystalline structure, and it is reported that the α-phase crystals of PA6 exhibit a higher modulus than the γ-phase.[29]

Conclusions

The presence of nanotubes increases the nucleation of the PA6, and therefore increases the temperature of crystallization of PA6. This rise in temperature is due to the formation of more perfect crystals generated for the presents of carbon nanotubes that act as nucleation agents.

When the carbon nanotubes are functionalized, $\Delta_m H$ of nanocomposites increases since there is a better interaction with the polymeric matrix and the polymer chains are immobilized. However, when the polymer chains and the fibers are very long, due to their high flexibility and a very high aspect ratio, they tend to be entangled, and the functionalization process can induce to their agglomeration. This causes a slight reduction in the nanocomposite's crystallinity because these agglomerates can hinder the diffusion and alignment of PA6 chains.

The silica nanoparticles reduce the temperature of crystallization of PA6 as the concentration of silica increases, while they increase considerably the thermal stability of nanocomposites when the silica is functionalized. This effect is more important in the composites with smaller particle size because more surface area is in contact.

Acknowledgements: We are grateful for financial support to: Universidad de Antioquia, Medellín and COLCIENCIAS, Bogotá, Colombia for the project with code 1115-06-17651

contract 216-2005 and also to the program "*Apoyo a la comunidad científica nacional a través de doctorados nacionales*"

[1] K. V. Katok, V. A. Tertykh, S. Ya. Brichka, G. P. Prikhod'ko, *Materials Chemistry and Physics* **2005**, *96*, 396.
[2] A. Huczko, *Appl. Phys. A* **2002**, *74*, 617.
[3] M. Corrias, Y. Kihn, P. Kalck, P. Serp, *Carbon* **2005**, *43*, 2817.
[4] K. Balasubramanian, M. Burghard, *small* **2005**, *1*, 180.
[5] V. N. Popov, *Materials Science and Engineering* **2004**, *R43*, 61.
[6] J. J. Rajesh, J. Bijwe, *Wear* **2005**, *259*, 661.
[7] M. Bermúdez, W. Brostow, F. J. Carrión, J. Cervnates, D. Pietkiewicz, *Polymer* **2005**, *46*, 347.
[8] J. J. Rajesh, J. Bijwe, U. S. Tewari, *Wear* **2002**, *252*, 769.
[9] T. D. Fornes, D. R. Paul, *Polymer* **2003**, *44*, 3945.
[10] T. Liu, I. Y. Phang, L. Shen, S. Y. Chow, W. Zhang, *Macromolecules* **2004**, *37*, 7214.
[11] W. Weng, G. Chen, D. Wu, *Polymer* **2003**, *44*, 8119.
[12] W. D. Zhang, L. Shen, I. Y. Phang, T. Liu, *Macromolecules* **2004**, *37*, 256.
[13] W. Shao, Q. Wang, F. Wang, Y. Chen, *Carbon* **2006**, *44*, 2708.
[14] J. Li, Z. Fang, L. Tong, A. Gu, F. Liu, *European Polymer Journal* **2006**, *42*, 3230.
[15] L. Qian, J. P. Hinestroza, *Journal of Textile and Apparel, Technology and Management* **2004**, *4*, 1.
[16] C. Zhao, G. Hu, R. Justice, D. W. Schaefer, S. Zhang, M. Yang, C. C. Han, *Polymer* **2005**, *46*, 5125.
[17] L. Qu, L. M. Veca, Y. Lin, A. Kitaygorodskiy, B. Chen, A. M. McCall, J. W. Connell, Y. P. Sun, *Macromolecules* **2005**, *38*, 10328.
[18] J. Gao, M. E. Itkis, A. Yu, E. Bekyarova, B. Zhao, R. C. Haddon, *J. Am. Chem. Soc.* **2005**, *127*, 3847.
[19] W. Stöber, A. Fink, E. Bohn, *J. Colloid Interface Sci.* **1968**, *26*, 62.
[20] H. Okudera, A. Hozumi, *Thin Solid Films* **2003**, *434*, 62.
[21] I. A. Rahman, P. Vejayakumaran, C. Sipaut, J. Ismail, M. Bakar, R. Adnan, C. Chee, *Colloids Surf. A.* **2007**, *294*, 102.
[22] D. Green, S. Jayasundara, Y. Lam, M. Harris, *Journal of Non-Crystalline Solids* **2003**, *315*, 166.
[23] Y. Yang, Z Hu Y. N. Lü Y. Chen, *Materials Chemistry and Physics* **2003**, *82*, 440.
[24] J. Cheng, X. Zhang, Z. Luo, F. Liu, Y. Ye, W. Yin, W. Liu, Y. Han, *Materials Chemistry and Physics* **2006**, *95*, 5.
[25] S. Reculusa, C. Mingotaud, E. Bourgeat, E. Duguet, S. Ravaine, *Nano Lett.* **2004**, *4*, 1677.
[26] G. Knowles, J. Graham, S. Delaney, A. Chaffe, *Fuel Processing Technology* **2005**, *86*, 1435.
[27] F. Yang, Y. Ou, Z. Yu, *Journal of Applied Polymer Science* **1998**, *69*, 355.
[28] S. S. Pesetskii, B. Jurkowski, Y. A. Olkhov, S. P. Bogdanovich, V. N. Koval, *European Polymer Journal* **2005**, *41*, 1380.
[29] D. M. Lincoln, R. A. Vaia, Z.-G. Wang, B. S. Hsiao, *Polymer* **2001**, *42*, 1621.

